Applied Catalysis A: General 358 (2009) 193–202

Pd/Ga_2O_3 methanol steam reforming catalysts: Part I: Morphology, composition and structural aspects

S. Penner[1,*], H. Lorenz[1], W. Jochum[1], M. Stöger-Pollach[2], D. Wang[3], C. Rameshan[1], B. Klötzer[1]

[1] Institute of Physical Chemistry, University of Innsbruck, Innrain 52a, A-6020 Innsbruck
[2] University Service Centre for Transmission Electron Microscopy (USTEM), Vienna University of Technology, Wiedner Hauptstrasse 8-10/052, A-1040, Vienna, Austria
[3] Fritz-Haber-Institut der Max-Planck-Gesellschaft, Faradayweg 4-6, D-14195 Berlin, Germany

[*] Corresponding author: e-mail simon.penner@uibk.ac.at,

Received: 14 September 2009, Accepted 12 February 2009, Published Online: 03 March 2009

Abstract

The combination of (High-resolution) electron microscopy, Selected Area Diffraction and X-ray Diffraction was applied to study the structural, compositional and morphological alterations of two Pd/Ga_2O_3 catalysts relevant for methanol steam reforming upon different oxidative and reductive treatments. These systems include well-defined Pd particles grown epitaxially on vacuum-cleaved NaCl(001) single crystals and subsequently covered by a layer of amorphous Ga_2O_3 (termed as "thin film model catalysts"), as well as, for comparison, a conventional Pd/Ga_2O_3 powder catalyst prepared by incipient wetness impregnation. Both catalysts were subsequently subjected to similar treatments in O_2 (1 bar, 1h) and H_2 (1 bar, 1h) in the temperature range between 373 and 923 K.

Oxidation of the thin film model catalyst at 773 K converts the Pd/Ga_2O_3 film into a mixture of PdO and Pd supported on Ga_2O_3. Subsequent reduction at 523 K causes the formation of an epitaxial Pd_5Ga_2 bimetallic phase with suppressed Pd hydride formation, in close correlation to the corresponding Pd/ZnO system. In contrast to the latter, Pd/Ga_2O_3 thin film model catalysts are prone to sintering at reduction temperatures $\geq$ 673 K. However, Pd_5Ga_2 with some Pd probably remaining in the particle cores is still present. The stability of the bimetallic Pd_5Ga_2 phase in oxygen was observed to depend on the prereduction history, that is, oxidation at 673 K of a bimetallic formed at 523 K causes the complete decomposition of the bimetallic phase and formation of PdO/Pd particles supported on Ga_2O_3, whereas bimetallics formed at higher reduction temperatures (i.e. $\geq$ 673 K) are only transformed back to Pd/Ga_2O_3. According to TEM investigations, this is due to the increased mobility of Ga and the subsequent formation of a Ga_2O_3 surface layer preventing further oxidation to PdO. Reduction of the corresponding Pd/β-Ga_2O_3 impregnated powder catalyst between 573 and 773 K causes the formation of a Pd_2Ga bimetallic phase, which is further converted to PdGa at reduction temperatures of 923 K. No formation of a Ga_2O_3 surface layer covering the particles has been observed upon reoxidation of the bimetallic. This is explained on the basis of the difference in metal (bimetallic)-support contact area.

Keywords: : Transmission electron microscopy, Selected area electron diffraction, Palladium, bimetallic particles, Pd_5Ga_2, X-ray diffraction, Pd_2Ga, PdGa

1. Introduction

The ability of different Pd/Ga_2O_3 samples to act as an efficient catalyst in methanol synthesis (from CO_2 and H_2) [1,2] and methanol steam reforming [3] is already well-established. Special attention has been focused on the identification of the catalytically active phase and key reaction intermediates [1-3]. Concerning methanol steam reforming, the catalytically active phase of Pd/Ga_2O_3 (and its ZnO and In_2O_3-supported counterparts) is usually regarded as an alloy phase formed after a pre-reductive treatment at temperatures between 523 and 773 K [3]. According to ref. [3], for the Pd/Ga_2O_3 system this alloy phase includes a mixture of Pd_5Ga_2 and $PdGa_5$, obtained after a reduction at 773 K. Although the corresponding Pd/ZnO system has attracted increased interest over the last few years from both the structural and catalytical point of view [4-8], especially structural information of the involved bimetallics in the

Pd/Ga_2O_3 system is still scarce. Structural information is basically limited to X-ray diffraction (XRD) measurements of Pd/Ga_2O_3 powder samples to reveal the eventual formation of the catalytically active Pd-Ga alloy(s) [3]. Despite the capabilities of modern transmission electron microscopy techniques, TEM studies of the Pd/Ga_2O_3 catalyst system regarding methanol steam reforming are virtually non-existent. In part this might be due to the Pd-Ga phase diagram [9], which appears to be significantly more complex compared to its ZnO-supported counterpart [10]. Concerning Pd/ZnO, the tetragonal PdZn bimetallic is easily obtained by reductive catalyst activation as a single phase and is indeed the most stable one as also observed in recent studies [3,7]. For Pd/ Ga_2O_3, the Pd-Ga phase diagram reveals a larger number of possible bimetallic structures in a close compositional range between 50 and 70 at.-% Pd. On top of this, some important ones (Pd_5Ga_2, Pd_2Ga and Pd_5Ga_3) exhibit very similar orthorhombic structures, which in turn leads to almost identical diffraction patterns [9,11-13]. Hence, preparation of a single bimetallic structure, phase determination and the identification of the catalytically active phase is not as straightforward as in the PdZn case.

Thus, the aim of this contribution and the adjoining paper dealing with the corresponding catalytic properties (part II, [14]) is the establishment of distinct structure-activity correlations in Pd/Ga_2O_3 methanol steam reforming catalyst systems. In the first place, this includes the preparation and structural characterization of a set of Pd/Ga_2O_3 catalysts which in turn will be converted into their possibly catalytically active phase by reductive activation. To induce the eventual formation of a single Pd-Ga bimetallic phase, two different preparation pathways, including the thin film model concept and studies on a "real", i.e. powder-supported Pd/Ga_2O_3 catalyst prepared by incipient wetness impregnation, will be followed. Concerning the first, this concept involves the epitaxial deposition of Pd particles onto vacuum-cleaved NaCl(001) single crystal planes and the subsequent embedding in a layer of Ga_2O_3. The main advantage of this concept, as it has been outlined in detail for similar Pt, Rh and Pd noble metal catalyst particles supported on different oxide supports [15-17], is that structural studies start from well-shaped and oriented epitaxial Pd particles which significantly facilitate not only investigations by TEM and related techniques, but also the subsequent establishment of structure-activity/selectivity correlations [15]. Moreover, the intimate contact between metal and oxide enhances the possible formation of a topotactic alloy triggered by the structure of the original metal catalyst particles [16]. For comparison, these studies are extended to a Pd/Ga_2O_3 powder catalyst, but in some more detail as examined originally by Iwasa et al [3].

Hence, the combination of both types of systems offers a functional approach to overcome the so-called "materials gap". On the other hand, as will be discussed in detail in section 3.3., it will also allow to assess the influence of the metal-support contact area on both structure and catalytic activity.

As bimetallic formation is considered as an extreme case of strong metal-support interaction (SMSI) [18], special attention will also be paid to other forms of SMSI-interaction between Pd and Ga_2O_3, such as e.g. decoration of Pd by reduced oxide species upon reduction.

High-resolution electron microscopy (HRTEM) and XRD as the most adequate tools for structural characterization are applied for phase determination. The results outlined in part I of the present contribution will hence serve as the "structural" basis for the discussion and the understanding of the catalytic results in methanol steam reforming highlighted in part II [14].

2. Experimental

A high-vacuum chamber (base pressure 10^{-4} Pa) was used to prepare the Ga_2O_3-supported Pd thin film model catalysts. For preparation of electron microscopy films, Pd metal was deposited by electron-beam evaporation onto a freshly-cleaved NaCl(001) plane at a base pressure of 10^{-4} Pa and a substrate temperature of 623 K (area of the NaCl single crystal about 0.25 cm^2). Subsequently, the Pd particles were covered by a layer of amorphous Ga_2O_3 (nominal thickness: 25nm), prepared by reactive deposition of Ga_2O_3 in 10^{-2} Pa O_2 at either 300 K or 600 K. As for the catalytic experiments in the micro-reactor larger-area samples are necessary to obtain sufficiently high conversion rates, thin films subsequently used for the catalytic experiments were prepared in the same experiment on freshly deposited NaCl thin films in a similar way as discussed above. The NaCl thin film supports were prepared by deposition of a polycrystalline NaCl thin film (thickness: 600 nm) at 298 K on two specially designed Cu sheets (37 cm^2 each). The structure of metal particles and support is almost identical on both substrates [19]. For subsequent structural characterization by electron microscopy, the resulting Pd/Ga_2O_3 films were floated and rinsed with distilled water, dried and finally mounted on gold grids. All films used for catalytic measurements were additionally covered by a supporting layer of amorphous SiO_2, prepared by reactive deposition of SiO in 10^{-2} Pa O_2 at 298 K (mean SiO_2 film thickness: 1000 nm). These films were subsequently floated in distilled water and thoroughly rinsed and dried before mounting on quartz wool inside the reactor.

The Pd/Ga_2O_3 powder catalyst was prepared by a standard incipient wetness technique. Ga_2O_3 powder (Alfa Aesar, 99.99%) was dispersed in ~150 ml distilled water and the Pd precursor ($Pd(NO_3)_2$ 99.95%, metals basis, 12 % Pd) was slowly added under permanent vigorous stirring. Finally, the water was evaporated and the resulting catalyst subjected to an oxidative treatment in air at 873 K for 1h. This procedure converts the catalyst into PdO/Ga_2O_3, as verified by routine X-ray diffraction measurements. X-ray photoelectron spectroscopy (performed at 300 K with a Thermo MultiLab 2000 spectrometer equipped with a

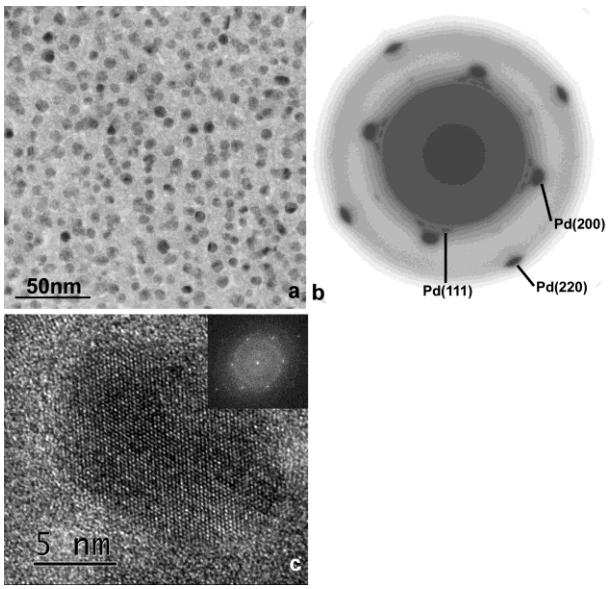

Fig. 1: (a) TEM overview image of as-deposited Pd particles supported on a Ga_2O_3 thin film, (b) corresponding SAED pattern, (c) high-resolution image of a single Pd particle oriented along a [110] zone axis (exhibiting (111) lattice spacings)

Table 1: Mean Pd (bimetallic) particle sizes on Pd/Ga_2O_3 and Pd/ZnO [7] thin film catalysts as deduced from TEM overview images.

Mean particle diameters of Pd/Ga_2O_3 and Pd/ZnO [7] catalysts upon reduction and bimetallics formation		
	Pd/Ga_2O_3 [nm]	Pd/ZnO [nm]
as grown	7.5	5.0
H-523 K	8.3	5.3
H-573 K	8.3	5.5
H-673 K	11.0	-
H-873 K	-	5.8

Mg/Al standard twin anode X-ray source using Al K_α radiation) was used to check the purity of these samples, but only showed peaks due to Pd, Ga and O with contaminants below the detection limit.

Reductive (1 bar H_2 for 1h), oxidative (1 bar O_2 for 1h) and tempering treatments in He (1 bar) were performed in parallel in a circulating batch reactor in the temperature range between 373-773 K. Structural and morphological changes were followed by (high-resolution) electron microscopy (HRTEM) and selected area electron diffraction (SAED). The electron micrographs were taken with either a ZEISS EM 10C, or with a Philips CM FEG 200 microscope and a 200 kV FEI TECNAI F20 S-TWIN Analytical (Scanning-) Transmission Electron Microscope (S)TEM. The film composition was checked by Energy-dispersive X-ray Spectroscopy (EDXS). Basically only peaks due to the evaporated elemental thin film constituents (Pd, Ga and O) and the gold grid (Au) were detected. Different amounts of Na (but always less than about 3%) were sometimes detected, too. However, Cl was never observed. The purity of the substrate was ensured by freshly cleaving the NaCl(001) crystals immediately before deposition of the oxide. The SAED patterns were calibrated with respect to the Pd spots in the untreated, as-grown state of the catalyst.

X-ray diffraction experiments were performed ex-situ under ambient conditions using a Siemens D5000 Spectrometer and Cu-K_α radiation (1.54178 Å) at 300 K.

3. Results and Discussion

3.1. Characterization of the as-grown catalysts

The as-grown state of the Pd/Ga_2O_3 thin film model catalyst (deposition temperature of Ga_2O_3 298 K), which will serve as the reference state for all structural investigations, is shown in Figure 1. Pd particles (Figure 1a; mean particle size: ~7.5 nm, see Table 1) are detected as black and grey dots. The black particles are in perfect Bragg-orientation, whereas the grey ones are slightly tilted out of their ideal Bragg position. The Ga_2O_3 support itself contributes only little to the TEM contrast, although sometimes grain boundaries in the support structure are observed. As it can be deduced from the SAED pattern (Figure 1b) and has also been the case for clean Ga_2O_3 [20], deposited at 298 K, the support is amorphous in the as-grown state and only reflections arising from the fcc structure of well-oriented Pd particles are visible. Some important diffraction spots have been marked. The SAED pattern indicates that most of the Pd particles are epitaxially aligned to the former NaCl(001) single crystalline substrate and are oriented along their [100] or [110] zone axes, giving rise to Pd (200)/Pd(220) and Pd(111) reflections, respectively. These observations are further corroborated by high-resolution imaging. Figure 1c shows a single Pd particle in [110] orientation (along with its Fast-Fourier Transform) with sets of (111) reflections rotated by 60° against each other.

XRD patterns of the Pd/Ga_2O_3 powder catalyst (bottom-most spectrum in Figure 8) indicate that its as-prepared state, i.e. after calcination in air at 873 K can be characterized as PdO/β-Ga_2O_3, i.e. according to TEM, small PdO particles are dispersed on large grains of β-Ga_2O_3. As will be discussed in detail in section 3.3.2., a reduction of the catalyst at 373 K (1 bar H_2, 1h) converts the PdO particles into metallic Pd. The so-obtained state of the powder catalyst hence will serve as a more convenient reference state especially for comparison of structural and catalytic changes (discussed in the subsequent paper [14]) with respect to the thin film model catalyst. This reference state of the Pd/Ga_2O_3 powder catalyst which can be seen in Figure 2a is characterized by a broader Pd particle-size distribu

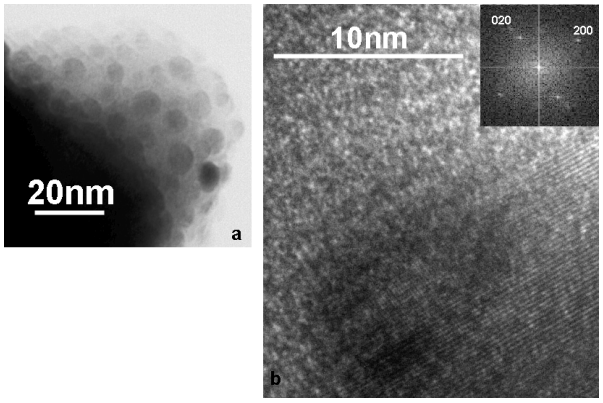

Fig. 2: TEM overview image of small Pd particles dispersed on a single β-Ga_2O_3 (a) and HRTEM image of a single metallic Pd particle in [100] orientation. [-111] lattice spacings of β-Ga_2O_3 are also observed (FFT is shown as an inset) (b).

tion. Pd particle sizes range from about 2 to 15 nm, with a mean particle diameter of about 7 nm, corresponding to a metal dispersion of 14 %. Some of the Pd particles exhibit quasi-hexagonal outlines, although most of them do have more irregular shapes. SAED patterns (not shown here) resemble Debye-Scherrer-type diffraction patterns due to the fact that - in contrast to the thin film model catalyst discussed above - the epitaxial alignment of the Pd (and PdO) particles is missing. Figure 2b shows a single Pd particle attached to a larger β-Ga_2O_3 grain. The Fast Fourier Transform (FFT) confirms that this particle is oriented along a [100] zone axis, that is, it exhibits two sets of perpendicular (200) lattice fringes measured at 1.95Å. A set of (-111) lattice fringes of the base-centered monoclinic β-Ga_2O_3 support structure [21] is visible in the lower right corner.

3.2. Oxidation of the Pd/Ga_2O_3 catalysts

In order to establish unambiguous structure-activity correlations, the structural alterations occuring both during oxidative and reductive catalyst activation treatments have to be appropriately assessed. This section therefore will highlight the structural and morphological changes on the Pd/Ga_2O_3 thin film catalysts resulting from oxidative treatments in the temperature range 373 K to 773 K.

At oxidation temperatures T ≤ 573 K, metallic Pd persists and no PdO formation is observed. Raising the oxidation temperatures to 673 K results in a partial conversion of Pd metal into PdO, as determined by the SAED pattern depicted in Figure 3b. PdO diffraction spots are observed and well-aligned to the corresponding Pd spots. This very much resembles the oxidation of Pd/SiO_2 catalysts, where a similar formation of epitaxial PdO has been observed [22]. Two major differences to Pd/SiO_2 are, however, worth to note. Firstly, although PdO formation sets in at roughly similar temperatures, no full transformation (as

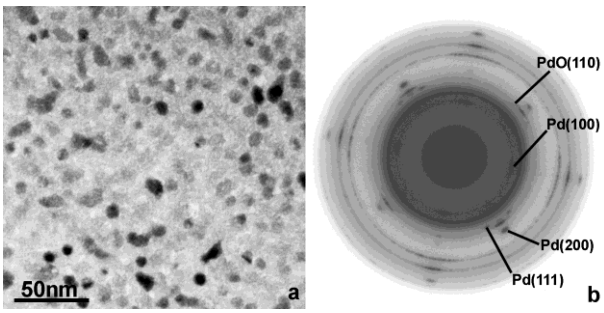

Fig. 3: (a) TEM overview image of the Pd/Ga_2O_3 thin film catalyst after oxidation at 673 K (1 bar O_2, 1h), (b) corresponding SAED pattern (some reflections of Pd and PdO have been marked).

in Pd/SiO_2) has been observed on Pd/Ga_2O_3, but only a mixture of Pd and PdO, even at the highest oxidation temperatures applied, i.e. 773 K. This is corroborated by the observation that the typical fragmented PdO particle structure observed on Pd/SiO_2 is almost entirely missing on Pd/Ga_2O_3. The origin of this differing behaviour is not entirely clear, but some of the results presented in the following provide evidence that at some point the oxidation pathway may become blocked due to inhibited diffusion of oxygen to metallic Pd.

3.3. Reductive bimetallic formation

3.3.1. Pd/Ga_2O_3 thin film

Figure 4 highlights the dependence of the particle structure on the pre-reduction temperature between 523 and 600 K. Below about 500 K, no change in particle structure, morphology or composition has been observed. After reduction at 523 K, a slight increase in particle size has been noted (mean particle size about 8.3 nm) without pronounced changes in the overall particle shapes (Figure 4a). Occasionally, coalescence phenomena are observed. As it was the case for the corresponding Pd/ZnO system [7], the SAED pattern already indicates a beginning structural and compositional transformation (Figure 4b). In addition to elongated diffraction spots arising from disoriented Pd particles, spots perfectly aligned to the Pd reflections appear. These new spots are found at distances d ~ 2.12, 2.04, 1.83 and 1.49 Å and are tentatively attributed to the (321), (002), (312) and (522) spots of the orthorhombic Pd_5Ga_2 structure [space group: Pbnm, a = 18.369, b = 5.485, c = 4.083 Å; d_{theor} (321) = 2.133 Å, d_{theor} (002) = 2.041Å, d_{theor} (321) = 1.826 Å, d_{theor} (522) = 1.495 Å] [11], which has also been observed by Iwasa et al. after a reduction of a Pd/Ga_2O_3 catalyst at 773 K in hydrogen [3].

It is worth to note, that a Pd/ZnO/SiO_2 catalyst reduced under similar experimental conditions exhibited the formation of a tetragonal PdZn bimetallic phase, also in epitaxial relation to the Pd lattice [7]. Similar results have

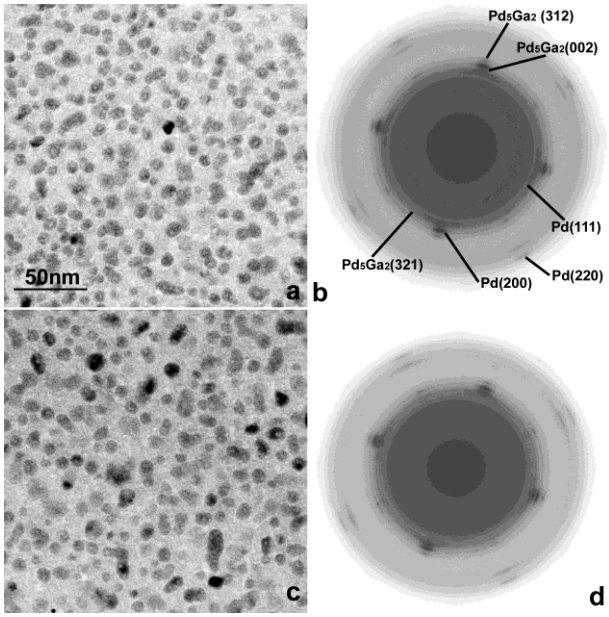

Fig. 4: TEM overview images of the Pd/Ga_2O_3 thin film catalyst after reduction (1 bar H_2, 1h) at 523 K (a) and 600 K (c). The corresponding SAED patterns are shown in (b) and (d).

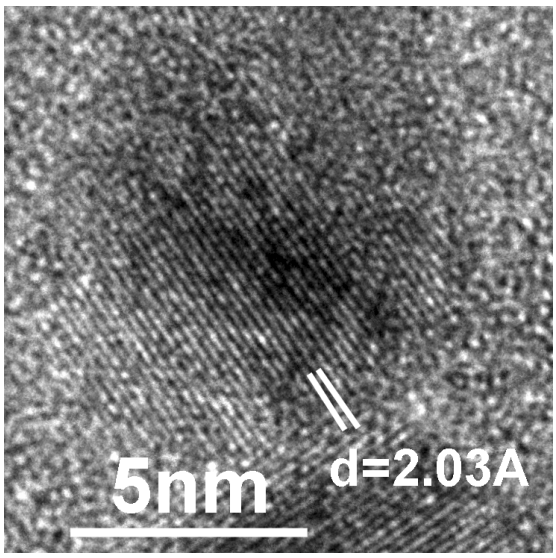

Fig. 5: High-resolution electron micrographs of (a) a single Pd particle exhibiting (111) lattice fringes and (b) a single Pd_5Ga_2 particle with (002) lattice fringes

been obtained for various oxide-supported Pt and Rh thin film catalysts [16]. As in these cases the topotactic formation of the bimetallic was attributed to a close matching of the Pd and the respective bimetallic structures, presumably a similar situation is present also for the Pd/Ga_2O_3 system, i.e. the formation of a specific bimetallic structure is driven by the good structural relation of the fcc Pd and, most probably, the Pd_5Ga_2 lattice. A word of caution should be added here: A close look at the phase diagrams of Pd-Zn and Pd-Ga reveals that in the former case, the 1:1 PdZn alloy with CuAu structure is not only the most stable, but also the one with the closest coincidence with the Pd fcc structure (a_{Pd}=3.89Å; a_{PdZn} = 4.10Å) [7]. The situation is much more complicated for the corresponding Pd-Ga system. The phase diagram reveals a set of thermodynamically stable structures (at least Pd_5Ga_2, Pd_5Ga_3, Pd_2Ga, PdGa with decreasing Pd content) in a small compositional range between 50 and 70% Pd. On top of this, Pd_5Ga_2, Pd_5Ga_3, Pd_2Ga all exhibit orthorhombic structures with somewhat similar lattice parameters (Pd_5Ga_3: a = 5.50Å, b = 10.53Å, c = 4.40Å; Pd_5Ga_2: see above; Pd_2Ga: a = 5.46Å, b = 4.03Å, c = 7.812Å) giving rise to very similar diffraction patterns [9,11-13]. The close structural relationship between especially Pd_5Ga_2 and Pd_2Ga has been outlined in detail by Khalaff et al. [11]. However, on the basis of a careful evaluation of the diffraction patterns from different, but similarly prepared samples, we dare to exclude Pd_2Ga, Pd_5Ga_3 and PdGa as possible present bimetallic phases, since reflections specific to these structures are clearly missing (e.g. the (301) reflection of Pd_2Ga or the (121) reflection of Pd_5Ga_3). This assumption is also feasible from the fact that most probably a Pd-richer bimetallic is formed at first (i.e. Pd_5Ga_2) and only at higher reduction tempera

tures diffusion of Ga is enhanced to eventually form more Pd-depleted Pd-Ga bimetallics. An overview of measured interplanar distances and their attribution to lattice spacings of Pd_5Ga_2 is given in Table 2.

Raising the reduction temperature to 573 K does not cause significant changes in particle structure or composition. No pronounced particle sintering has been observed (mean particle size about 8.3 nm; Figure 4c) and also the SAED pattern (Figure 4d) shows no additional reflections. Most importantly, as in the case of Pd/ZnO, up to 573 K Pd-hydride formation is suppressed [7, 23].

HRTEM imaging basically confirms the presence of Pd_5Ga_2. Figure 5 shows a single Pd_5Ga_2 particle (after reduction at 523 K) exhibiting lattice fringes of about 2.03Å, which most probably can be attributed to the (002) spacings of the orthorhombic Pd_5Ga_2 structure. It should be noted that after reduction at 523 K some Pd particles can still be detected.

More pronounced changes also inducing major catalytic consequences (as discussed in part II of the present contribution [14]) are observed upon raising the reduction temperature to 673 K. As obvious from Figure 6a, the mean diameter of the particles has now significantly increased to about 11.3 nm (compared to only about 5.8 nm after reduction at 873 K from 5.0 nm in the as-grown state determined on Pd/ZnO) with most of the particles exhibiting round shapes. The SAED pattern (Figure 6b) reveals two additional reflections at around 2.34 and 2.43Å, which can be attributed to the (420) [d_{theor}(420) = 2.354Å] and (511) lattice spacings [d_{theor}(511) = 2.444Å] of orthorhombic Pd_5Ga_2. These two reflections have also been observed on some samples even after reduction at 523 K. We therefore conclude that at 523 and 673 K the same Pd_5Ga_2 structure in sometimes slightly different orientations is present with variable amount. Both other structures (Pd_2Ga and Pd_5Ga_3)

Table 2: Interplanar distances d_{hkl} [Å] measured on the Pd/Ga_2O_3 thin film after different reduction steps and possible correlation to cubic Pd metal and the orthorhombic Pd_5Ga_2 alloy phase

Pd–Ga as-grown			Pd–Ga H-523 K			Pd–Ga H-673 K		
	Assignment			Assignment			Assignment	
$d(h\,k\,l)_{exp}$	$d(h\,k\,l)_{theor}$	Lattice plane	$d(h\,k\,l)_{exp}$	$d(h\,k\,l)_{theor}$	Lattice plane	$d(h\,k\,l)_{exp}$	$d(h\,k\,l)_{theor}$	Lattice plane
2.24	2.245	Pd(1 1 1)	2.24	2.245	Pd(1 1 1)	2.43	2.444	Pd_5Ga_2(5 1 1)
1.96	1.945	Pd(2 0 0)	2.12	2.133	Pd_5Ga_2(3 2 1)	2.34	2.354	Pd_5Ga_2(4 2 0)
						2.23	2.245	Pd(1 1 1)
1.36	1.370	Pd(2 2 0)	2.04	2.042	Pd_5Ga_2(0 0 2)	2.12	2.133	Pd_5Ga_2(3 2 1)
				2.042	Pd_5Ga_2(4 2 1)			
				2.047	Pd_5Ga_2(7 1 1)	1.96	1.945	Pd(2 0 0)
			1.96	1.945	Pd(2 0 0)	1.89	1.896	Pd_5Ga_2(7 2 0)
			1.83	1.826	Pd_5Ga_2(3 1 2)	1.83	1.826	Pd_5Ga_2(3 1 2)
				1.837	Pd_5Ga_2(10 0 0)		1.837	Pd_5Ga_2(10 0 0)
			1.49	1.495	Pd_5Ga_2(5 2 2)	1.64	1.641	Pd_5Ga_2(2 3 1)
				1.487	Pd_5Ga_2(11 1 1)			
						1.49	1.495	Pd_5Ga_2(5 2 2)
			1.37	1.370	Pd(2 2 0)		1.487	Pd_5Ga_2(11 1 1)
						1.36	1.370	Pd(2 2 0)

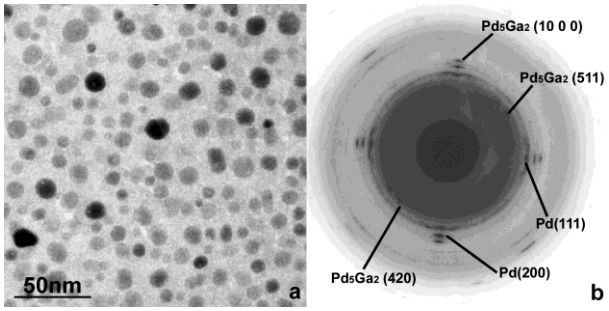

Fig. 6: TEM overview images of the Pd/Ga_2O_3 thin film catalyst after reduction (1 bar H_2, 1h) at 673 K (a). The corresponding SAED patterns are shown in (b)

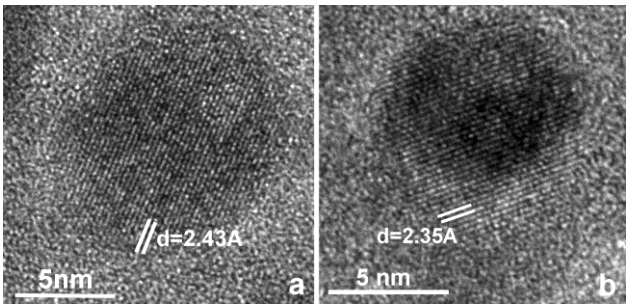

Fig. 7: High-resolution electron micrographs of (a) a single Pd_5Ga_2 particle exhibiting (511) lattice fringes and (b) a single Pd_5Ga_2 particle with (420) lattice fringes.

do not match these lattice spacings appropriately [12,13]. Details of the correlation of experimental and theoretical interplanar distances are given in Table 2. Since the intensity of the metallic Pd spots has decreased significantly (and vice versa the intensity of the bimetallic spots increased), we conclude that most of the particles now consist of Pd_5Ga_2 with some Pd remaining likely in the particle cores.

Figure 7 highlights two single Pd_5Ga_2 particles with (420) and (511) lattice spacings (Figure 7a and b, respectively). We note two differences to the corresponding Pd/ZnO-System: Firstly, according to the SAED pattern shown in Figure 6b, Pd metal is still present after reduction at 673 K (for Pd/ZnO a complete transformation into PdZn has been observed at this temperature). Secondly, as Pd/Ga_2O_3 is prone to considerable sintering at 673 K, no "strong particle stabilization effect", a term coined for the structural and morphological high-temperature stability of Pd/ZnO under reductive and reactive environments [7], has been observed for Pd/Ga_2O_3. As highlighted in detail for example for the Pt/SiO_2 system in a previous publication, the first part of the topotactic alloy formation involves considerable reduction of the supporting oxide in the presence of a noble metal capable of dissociative hydrogen adsorp tion [16, 24]. We might therefore anticipate that a similar process is operative for the Pd/Ga_2O_3 system, which involves reduction of Ga_2O_3 to highly mobile Ga_2O or other sub-oxidic Ga-species and the subsequent diffusion of Ga into Pd to form the Pd-Ga alloy. In support of this "sub-oxide-mediated" growth mechanism we note that a thermal annealing treatment in pure He at 673 K similarly results in the formation of the Pd_5Ga_2 alloy phase and SAED patterns very closely resemble the ones obtained after a reductive treatment in 1 bar H_2 at 523 K.

3.3.2. Pd/Ga_2O_3 powder catalyst

In order to close the "materials gap", a corresponding Pd/Ga_2O_3 powder catalyst prepared via incipient wetness impregnation has been treated and analyzed in a similar way as the thin film discussed above.

Figure 8 shows a set of XRD spectra taken at different stages of reduction between 373 and 923 K. The bottom-most spectrum corresponds to the as-prepared catalyst after oxidation at 873 K and accordingly shows only peaks arising from the tetragonal PdO phase [25] and the base-

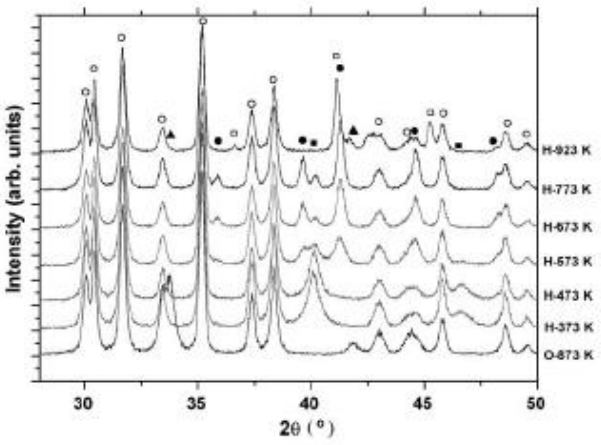

Fig. 8: Set of XRD spectra taken on the Pd/Ga_2O_3 powder catalyst after different treatments in O_2 and H_2. Bottom-most spectrum: as-prepared catalyst corresponding to oxidation at 873 K, top-most spectrum: after reduction at 923 K. (●)...orthorhombic Pd_2Ga, (▲)...cubic PdO, (■)....fcc Pd, (□)...cubic PdGa, (○)...base-centered monoclinic β-Ga_2O_3.

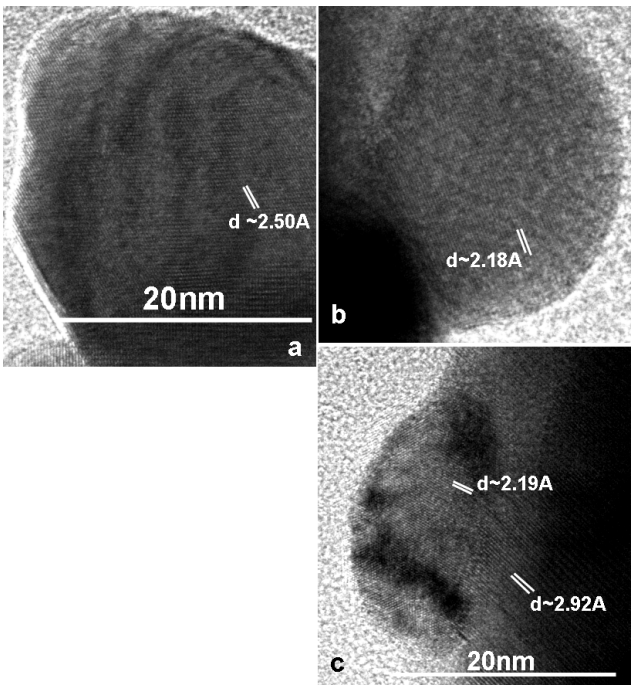

Fig. 9: High-resolution TEM images of single alloy particles obtained after reduction at 773 K and 923 K: (a) Pd_2Ga [(121) lattice fringes], (b) Pd_2Ga [(211) lattice fringes] and (c) PdGa [(012) lattice fringes]

centered monoclinic structure of β-Ga_2O_3 [21]. No peaks arising from the fcc structure of Pd are visible. However, as already indicated above, a reductive treatment at 373 K or 473 K causes a complete transformation of PdO/β-Ga_2O_3 into Pd/β-Ga_2O_3. Additional peaks start to appear around 573 K reduction temperature (marked by (●) in Figure 8). Up to 773 K reduction temperature, these peaks increase and correspondingly, the Pd peaks are decreased. Hence, even at 773 K, metallic Pd is still present and no complete phase transformation towards bimetallic phases takes place. All the additional peaks (measured at d = 2.502, 2.271, 2.184, 2.029, 1.884 and 1.381 Å) can be attributed to the orthorhombic Pd_2Ga structure [d_{theor}(211) = 2.501Å, d_{theor}(021) = 2.271Å, d_{theor}(301) = 2.184Å, d_{theor}(002) = 2.028Å, d_{theor}(320) = 1.886Å, d_{theor}(322) = 1.381Å] [13]. An important note should be added at this stage, that is, in contrast to the thin film samples, Pd_2Ga is almost exclusively formed instead of Pd_5Ga_2 and, in contrast to Iwasa et al., who report both Pd_5Ga_2 and the much Ga-richer $PdGa_5$ after a reduction at 773 K [5]. An explanation on the basis of the excellent epitaxy between Pd and the resulting bimetallic phase appears likely. Since for the preparation of the thin film epitaxially grown Pd particles are covered by Ga_2O_3 we may safely assume that the structure of Pd triggers the formation of the bimetallic with the best-fit structure relative to the structure of the original Pd lattice. This need not primarily be the thermodynamically *most* stable one (Pd_2Ga in this case). A similar situation has been present e.g. for the Pt/SiO_2 catalyst. Although PtSi and Pt_2Si are the thermodynamically most stable bimetallics, formation of Pt_3Si (with almost perfect epitaxy to Pt) has exclusively been observed [24]. The structural match between Pd and Pd_5Ga_2, better than with Pd_2Ga, is probably still close enough to induce the predominant formation of Pd_5Ga_2. As this epitaxy is not relevant in the case of the powder catalyst, exhibiting a largely irregular arrangement of grains and particles, one would expect the formation of the thermodynamically most stable bimetallic, which is Pd_2Ga if no major limitations of its growth are present. It should be also noted, that the metal dispersion of the catalyst decreases to about 4 % after reduction at 773 K.

Raising the reduction temperature to 923 K (top-most spectrum) causes a transformation of the Pd_2Ga structure into the more Ga-richer PdGa alloy phase. These new spots have been marked by open squares in Figure 9. Peaks are observed at d =3.471Å, 2.451Å, 2.194Å and 2.002Å. (all other peaks either belong to β-Ga_2O_3 or the sample holder). These spacings can be attributed to the (110), (200), (012) and (211) spacings of the cubic PdGa structure [d_{theor}(110) = 3.458Å; d_{theor}(200) = 2.445Å; d_{theor}(012) = 2.186Å; d_{theor}(211) = 1.996Å] [12]. We observe a small deviation from the calculated spectrum, but this might be due to a slightly distorted PdGa lattice. No signals of metallic Pd or Pd_2Ga are remaining.

Selected HRTEM images of the catalyst after different stages of reduction are shown in Figure 9. These findings basically confirm the evaluation of the XRD patterns and show some Pd_2Ga (Figure 9a and b) and mainly PdGa (Figure c) after reduction at 773 K and 923 K, respectively. Figure 9a and b highlight bimetallic particles with (121) (measured: 2.50Å; theoretical: 2.50Å) and (211) fringes (measured: 2.18Å; theoretical: 2.18Å) of the orthorhombic Pd_2Ga structure, whereas a single PdGa particle exhibiting (012) lattice fringes is depicted in Figure 9c (measured: 2.19Å; theoretical: 2.19Å). (-401) lattice spacings (measured: 2.92Å; theoretical: 2.93Å) of the β-Ga_2O_3 structure are additionally visible.

The $PdGa_5$ structure reported by Iwasa et al. [3] was never observed throughout the whole temperature series of reduction experiments reported here, likely because extreme reduction conditions are required to induce such an extremely Ga-rich bimetallic species.

3.3.3. Stability of the Pd-Ga alloys under oxidative conditions

The stability of the alloys formed on both the thin film and the powder samples have subsequently been tested under oxidative environments as this is of crucial importance of oxidative catalyst regeneration. As in our case the life-cycle of the catalyst usually involves the reductive formation of the potentially catalytically active (bimetallic) phase starting from a defined, oxidized initial state and a subsequent methanol steam reforming reaction, the conditions for an effective oxidative regeneration treatment that regenerates the initial state are of special interest. Therefore, we subjected both catalysts after different stages of reduction (= different extent of bimetallic formation) to similar oxidative treatments.

Concerning the thin film model catalyst, reduction was carried out at 523 K and 673 K respectively, and afterwards both catalysts were subjected to oxidation between 373 and 673 K (1 bar O_2, 1h). At and below 473 K, the bimetallic formed on both samples was stable and no decomposition was observed. First differences were noted upon raising the re-oxidation temperature to 573 K, at which temperature the bimetallic formed at 673 K proved to be still stable, whereas on the catalyst reduced at 523 K formation of a mixture of Pd and PdO has been observed (not shown here). Figure 10 finally highlights the state of the catalysts after an oxidative treatment at 673 K. Both Pd and PdO are observed on the catalyst reduced at 523 K (Figure 10 a, b). In contrast, on the catalyst subjected to pre-reduction at 673 K - although the bimetallic has completely decomposed according to the SAED pattern - only metallic Pd is present. In both cases, no re-dispersion of the catalyst particles has been observed.

How to understand this qualitatively different behavior? A close look at the TEM image of Figure 10c reveals a shell around almost every Pd (or bimetallic) particle which is exclusively observed if the catalyst has been reduced at temperatures $T \geq 673$ K and subsequent oxidation at 673 K. Although the thin film catalyst a priori is not ideally suited for detection of particle overlayer structures due to plane-view imaging, we address this surrounding structure to a Ga_2O_3 layer covering the Pd particles. This is also indirectly proven by the catalytic experiments outlined in part II of the present contribution [14], where a switch from CO_2-selective methanol steam reforming after reduction at temperatures $T < 673$ K to the activity and selectivity pattern typical for clean β-Ga_2O_3 (i.e. after reduction at 673 K followed by oxidation at 673 K no Pd-related active

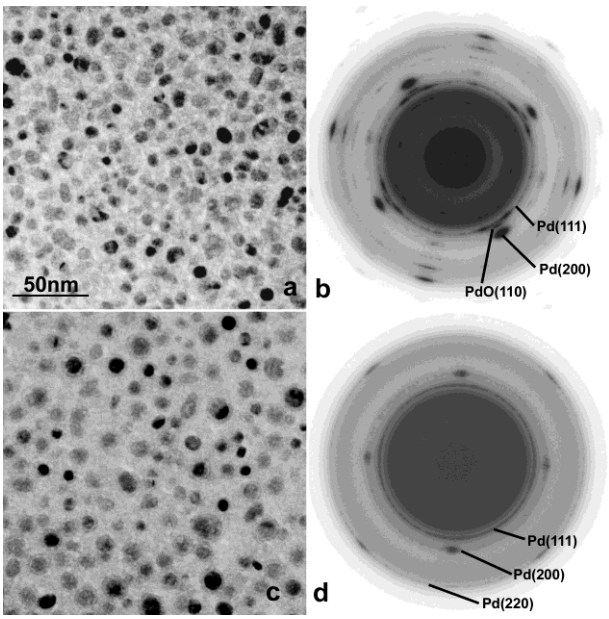

Fig. 10: TEM overview images of the Pd/Ga_2O_3 thin film catalyst after reduction (1 bar H_2, 1h) at 523 K (a) and 673 K (c) followed by *subsequent* re-oxidation at 673 K (1 bar O_2, 1h). The corresponding SAED patterns are shown in (b) and (d).

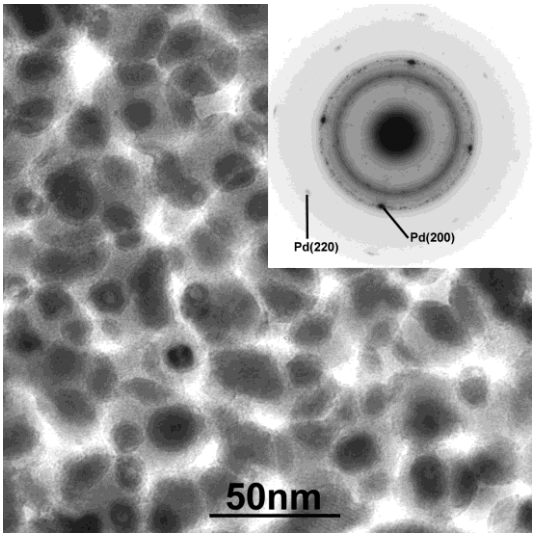

Fig. 11: TEM overview images of the as-grown Pd/Ga_2O_3 thin film model catalyst prepared by depositing the Ga_2O_3 supporting layer at 600 K. The corresponding SAED pattern is shwon as an inset.

ty has been observed (see Figure 5 of ref. [14]) suggesting complete deactivation of Pd by a Ga_2O_3 skin. How this layer is exactly formed remains unclear, but might be understood in terms of segregation of Ga to the surface of the bimetallic particles upon beginning decomposition of the bimetallic at 673 K, thus forming a Ga-rich overlayer which in turn is converted into β-Ga_2O_3 by oxidation at 673 K. Thus, the diffusion of O_2 and also of the steam reforming reactants to the bimetallic (or Pd) particles is blocked, at least at the oxidation temperatures applied.

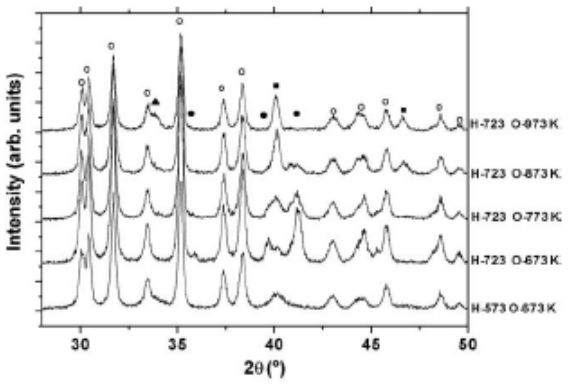

Fig. 12: Set of XRD spectra taken on the Pd/Ga_2O_3 powder catalyst after re-oxidation treatments in O_2 after different treatments in H_2. Bottom-most spectrum: reduction at 573 K, re-oxidation at 673 K top-most spectrum: reduction at 723 K, re-oxidation at 973 K. (●)...orthorhombic Pd_2Ga, (▲)...cubic PdO, (■)....fcc Pd, (○)...base-centered monoclinic β-Ga_2O_3.

The presence of a β-Ga_2O_3 skin is also corroborated by an additional thin film experiment, where the Pd particles were embedded in a β-Ga_2O_3 support at 600 K substrate temperature (Figure 11) and 10^{-2} Pa O_2 background pressure. The catalyst is characterized by large rounded gallia grains (as discussed in ref. [20] for clean β-Ga_2O_3) which are decorated by smaller dark Pd particles, each of which show the same core-shell structure as discussed above. According to ref. [20], at 600 K NaCl substrate temperature mobile sub-oxidic GaO_x species (which subsequently become oxidized in the background O_2 pressure toward Ga_2O_3) are mobile enough to cover the Pd particles. The SAED pattern basically only shows strong reflections of the fcc Pd structure since β-Ga_2O_3 remains quasi-amorphous even at 600 K substrate temperature.

A qualitatively similar scenario concerning re-oxidation as a function of pre-reduction temperature has been observed for the powder catalyst. The results are highlighted in Figure 12. Depending on the pre-reduction temperature, more or less severe oxidative treatments were necessary to decompose the alloys into Pd and/or PdO. After reduction at 573 K, comparably mild re-oxidation treatments at 673 K were sufficient to cause the formation of metallic Pd (bottom-most spectrum in Figure 12). After a pre-reduction at 723 K, a slight decrease of the peaks arising from Pd_2Ga has been observed at re-oxidation temperatures between 673 and 773 K. Even after oxidation at 873 K, some Pd_2Ga is still present. Oxidation temperatures of 973 K are necessary to fully decompose the remaining Pd_2Ga bimetallic and only peaks due to metallic Pd (and β-Ga_2O_3; we note also one small peak due to PdO) are observed in the XRD spectrum. The relatively sharp Pd (111) peak indicates rather large Pd particles.

4. Conclusions

In conclusion we note that, although bimetallic formation on Pd/Ga_2O_3 and their Pd/ZnO counterpart start at almost the same temperature and Pd hydride formation is suppressed on both catalysts, which in turn leads to a very similar catalytic behaviour, some differences in structure, morphology and composition have to be considered. Concerning the thin film systems, this essentially refers to the formation of a Pd_5Ga_2 alloy phase (PdZn is observed for Pd/ZnO) and the sintering effects of the bimetallic phases above reduction temperatures T = 673 K. Discussions about structure-activity correlations will also have to include the potential quasi-SMSI behaviour of β-Ga_2O_3 at higher reduction temperatures and its consequences for catalytic activity, selectivity and regeneration. The comparison of both Pd/Ga_2O_3 catalysts (thin film versus powder) shows the importance of the metal (or bimetallic)/support interface in the formation of the potentially catalytically active phase and further underlines the validity of the thin film model concept that allows a straightforward characterization of the catalyst structure without being too far away from a real catalysts' scenario.

Acknowledgements

We thank the FWF (Austrian Science Foundation) for financial support under the project P208920-N19.

References

[1] T. Fujitani, M. Saito, Y. Kanai, T. Watanabe, J. Nakamura, T. Uchijima, Appl. Catal. A 125 (1995) L199
[2] S. E. Collins, M. A. Baltanas, A. L. Bonivardi, J. Catal. 226 (2004) 410
[3] N. Iwasa, T. Mayanagi, N. Ogawa, K. Sakata, N. Takezawa, Catal. Lett. 54 (1998) 119
[4] A. Karim, T. Conant, A. Datye, J. Catal. 243 (2006) 420
[5] N. Iwasa, N. Takezawa, Top. Catal. 22 (2003) 215
[6] H. Gabasch, A. Knop, R. Schlögl, S. Penner, B. Jenewein, K. Hayek, B. Klötzer, J. Phys. Chem. 110 (23) (2006) 11391
[7] S. Penner, B. Jenewein, H. Gabasch, B. Klötzer, D. Wang, A. Knop, R. Schlögl, K. Hayek, J. Catal. 241 (2006) 14
[8] A. Bayer, K. Flechtner, R. Denecke, H. P. Steinrück, K. M. Neymann, N. Rösch, Surf. Sci. 600 (2006) 78
[9] Landolt- Börnstein, *Phase equilibria, Crystallographic and Thermodynamic Data of Binary Alloys*, Subvolume F, Springer, Berlin 1996

[10] Landolt- Börnstein, *Phase equilibria, Crystallographic and Thermodynamic Data of Binary Alloys*, Subvolume I, Springer, Berlin 1996
[11] K. Khalaff, K. Schubert J. Less. Common Metals 37 (1974) 129
[12] M. K. Bhargava, A. A. Gadalla, K. Schubert, J. Less. Common Metals 42 (1975) 69
[13] K. Schubert, H. L. Lukas, H.-G. Meissner, S. Bahn, Z. Metallkd. 50 (1959) 534
[14] H. Lorenz, S. Penner, W. Jochum, B. Klötzer, following paper
[15] G. Rupprechter, K. Hayek, L. Rendon, J. M. Yacaman, Thin Solid Films 260 (1995) 148
[16] S. Penner, D. Wang, D. S. Su, G. Rupprechter, R. Podloucky, R. Schlögl, K. Hayek Surf. Sci 532-535 (2003) 276
[17] S. Penner, D. Wang, R. Schlögl, K. Hayek Thin Solid Films 484 (2005) 10
[18] S. J. Tauster, S. C. Fung, R. L. Garten, J. Am. Chem. Soc. 100 (1978) 170
[19] G. Rupprechter, K. Hayek, H. Hofmeister, J. Catal. 173 (1998) 409
[20] S. Penner, B. Klötzer, B. Jenewein, F. Klauser, X. Liu, E. Bertel, Thin Solid Films 516 (2008) 4742
[21] D. Grier, G. McCarthy, North Dakota State University, Fargo, North Dakota, USA, ICDD Grant-in-Aid 1991; Powder Diffraction File, International Center for Diffraction Data 1994, pattern 00-043-1012
[22] S. Penner, D. Wang, B. Jenewein, H. Gabasch, B. Klötzer, A. Knop, R. Schlögl, K. Hayek, J. Chem. Phys. 125 (2006) 094703
[23] B. Jenewein, S. Penner, H. Gabasch, B. Klötzer, D. Wang, A. Knop, R. Schlögl, K. Hayek, J. Catal. 241 (2006) 155
[24] D. Wang, S. Penner, D. S. Su, G. Rupprechter, K. Hayek, R. Schlögl, J. Catal. 219 (2003) 434
[25] Powder Diffraction File, International Center for Diffraction Data 2005, pattern 00-006-0515